Eco-Environment & Health 2 (2023) 278–286

Contents lists available at ScienceDirect

Eco-Environment & Health

journal homepage: www.journals.elsevier.com/eco-environment-and-health

Original Research Article

Insights into the enzymatic degradation of DNA expedited by typical perfluoroalkyl acids

Chao Qin [a,b], Run-Hao Zhang [a], Zekai Li [b], Hai-Ming Zhao [a], Yan-Wen Li [a], Nai-Xian Feng [a], Hui Li [a], Quan-Ying Cai [a], Xiaojie Hu [b], Yanzheng Gao [b], Lei Xiang [a,*], Ce-Hui Mo [a,*], Baoshan Xing [c]

[a] Guangdong Provincial Research Center for Environment Pollution Control and Remediation Materials, College of Life Science and Technology, Jinan University, Guangzhou 510632, China
[b] Institute of Organic Contaminant Control and Soil Remediation, College of Resources and Environmental Sciences, Nanjing Agricultural University, Nanjing 210095, China
[c] Stockbridge School of Agriculture, University of Massachusetts, Amherst, MA 01003, United States

ARTICLE INFO

Keywords:
DNA
Enzymatic degradation
Emerging organic pollutants
Perfluoroalkyl acids
Ecological effects

ABSTRACT

Perfluoroalkyl acids (PFAAs) are considered forever chemicals, gaining increasing attention for their hazardous impacts. However, the ecological effects of PFAAs remain unclear. Environmental DNA (eDNA), as the environmental gene pool, is often collected for evaluating the ecotoxicological effects of pollutants. In this study, we found that all PFAAs investigated, including perfluorohexanoic acid, perfluorooctanoic acid, perfluorononanoic acid, and perfluorooctane sulfonate, even at low concentrations (0.02 and 0.05 mg/L), expedited the enzymatic degradation of DNA in a nonlinear dose–effect relationship, with DNA degradation fragment sizes being lower than 1,000 bp and 200 bp after 15 and 30 min of degradation, respectively. This phenomenon was attributed to the binding interaction between PFAAs and AT bases in DNA via groove binding. van der Waals force (especially dispersion force) and hydrogen bonding are the main binding forces. DNA binding with PFAAs led to decreased base stacking and right-handed helicity, resulting in loose DNA structure exposing more digestion sites for degrading enzymes, and accelerating the enzymatic degradation of DNA. The global ecological risk evaluation results indicated that PFAA contamination could cause medium and high molecular ecological risk in 497 samples from 11 contamination-hot countries (such as the USA, Canada, and China). The findings of this study show new insights into the influence of PFAAs on the environmental fates of biomacromolecules and reveal the hidden molecular ecological effects of PFAAs in the environment.

1. Introduction

Perfluoroalkyl acids (PFAAs), as chain-like ionic emerging pollutants rich in C–F bonds (116 kcal/mol), are difficult to hydrolyze, photolyzed, or degrade by microorganisms after entering the environment [1,2]. They are considered forever chemicals and can lead to long persistence and wide distribution in various environmental media [3]. PFAAs are gaining attention for their hazardous impacts, e.g., cytotoxicity, aquatic toxicity, embryotoxicity, hepatotoxicity, immunotoxicity, etc. Some previous studies have demonstrated the genotoxic effects of PFAAs in living cells. For example, PFAAs can induce double-strand breaks of intracellular DNA in HepG2 cells [4], sperm DNA methylation [5], chromosomal breakage [6], DNA instability [7], DNA damage [8], and changes in thyroid-related gene expression [9]. However, no investigation of their *in vitro* molecular ecological effect, such as the influence on DNA enzymatic degradation, has yet been reported, since the previous studies focused mainly on the toxicologic effects of PFAAs *in vivo*. A pioneering study demonstrated that a typical PFAA [i.e., perfluorooctane sulfonic acid (PFOS)] can bind to the groove bases of DNA duplexes [10]. However, quantitatively decomposing interaction energies between PFAAs and DNA is challenging, since PFAAs containing C–F bonds exhibit complex halogen-bonding dispersion interactions, which are difficult to assess via standard reduced density gradient calculations. In addition, whether the interaction between PFAAs and DNA will lead to further molecular ecological effects requires further investigation.

Environmental DNA (eDNA) often derives from bacterial secretions released from membrane vesicles [11]. There is the ubiquitous

* Corresponding authors.
E-mail addresses: xianglei@jnu.edu.cn (L. Xiang), tchmo@jnu.edu.cn (C.-H. Mo).

https://doi.org/10.1016/j.eehl.2023.09.002
Received 2 June 2023; Received in revised form 27 August 2023; Accepted 5 September 2023
Available online 17 September 2023

occurrence of eDNA, with an abundance of 70 μg/L, 17 μg/L, 2 mg/kg, and 6 mg/kg in freshwater, seawater, sediment, and soil, respectively [11,12]. eDNA can serve as a nutritional source for environmental microorganisms, an aggregate stabilizing agent in biofilms, and a selective plant allelopathic substance in the environment [13–15]. More importantly, eDNA often contains genetic information that can be integrated into the genomes of bacteria, leading to niche expansion and a competitive advantage against other organisms within their environment [16]. With its unique base sequences and genetic information storage functions, eDNA is referred to as the "environmental gene pool" [17,18]. The increased environmental pollution has led to the co-existence of pollutants with eDNA. Therefore, eDNA exposed to the natural environment is often collected for monitoring the biodiversity of the ecosystem to effectively evaluate the ecotoxicological effects of chemical contamination [19]. Especially, the degradation of eDNA induced by a pollutant and the subsequent potential release of the toxic genes carried by the eDNA can be considered an indicator for the ecotoxicological effects of the pollutant [20,21]. However, how much ecological risk is triggered by the pollutants-eDNA interactions remains a large knowledge gap for humans, although sporadic studies have reported that concomitant organic pollutants (e.g., bromobenzene, chlorobenzene, phenanthrene, pyrene, neomycin B, and chlorpyrifos) can affect DNA degradation [22–26]. Furthermore, wide variability in DNA degradation mechanism estimates currently exists in the published literature. Besides, the impacts and mechanism of the chain-like ionic organic emerging pollutants (PFAAs) on DNA degradation have not yet been reported.

In this study, gel electrophoresis, ultraviolet–visible spectroscopy, and atomic force microscopy (AFM) were performed to complete qualitative and quantitative assessment of DNA enzymatic degradation influenced by PFAAs. Salmon sperm DNA and four typical PFAAs with different carbon chain lengths and functional group substitutions [perfluorohexanoic acid (PFHxA), perfluorooctanoic acid (PFOA), perfluorononanoic acid (PFNA), and PFOS] were, respectively, selected as representative eDNA and PFAAs. Furthermore, the mechanisms underlying PFAA effects on DNA degradation can be clarified through fluorescence titration tests, Fourier-transform infrared spectra, circular dichroism (CD), and quantum chemical calculations. In particular, the quantitative decomposition of the interactions between DNA and PFAAs was performed by symmetry-adapted perturbation theory (SAPT). Based on the effects of PFAAs on DNA degradation and the global data on PFAA concentration in water, the global ecological risk evaluation of PFAAs was also conducted. This work highlights the profound effects of PFAAs on DNA degradation, clarifying the molecular ecological effects and risk of PFAAs contamination.

2. Materials and methods

2.1. DNA degradation experiments

Salmon sperm DNA has a double-stranded B-DNA structure composed of four types of nucleotides (A, T, G, and C), and it is widely used as the representative DNA in the environment for various studies, including its binding interaction with organic pollutants [27,28], adsorption on clay minerals [29,30], and aggregation in water environment [31,32]. This kind of DNA is, therefore, selected in this study. Deoxyribonuclease I (DNase I) is a representative degrading enzyme of extracellular DNA [33]. It can catalyze the hydrolysis of the phosphodiester bond between the phosphate group and the deoxyribose part of DNA, forming oligonucleotides with 5′-phosphates and 3′-phosphates [34], and is thus selected in this study.

Gel electrophoresis tests were conducted to visualize the degradation process of DNA affected by PFHxA, PFOA, PFNA, and PFOS (Sigma-Aldrich). First, PFAA–DNA mixtures were obtained through separate additions of 2 mg/L stock solutions of each PFAA to 500 mg/L DNA stock solution. The resulting mixtures were diluted with 10 mmol/L Tris–HCl (pH 7.4, Solarbio, Beijing, China), shaken at 120 r/min, and then stored in a refrigerator at 4 °C for 2 h. Next, the mixtures were treated with DNase I (Kangwei Century, Taizhou, Jiangsu, China) for DNA degradation. Mixed samples of the same concentrations without DNase I were used as blank controls. In the degradation reaction mixtures, concentrations of DNA and DNase I were set to 100 mg/L and 0.002 U/μL, respectively. Meanwhile, a series of concentrations of PFAAs were used, including 0, 0.02, 0.05, 0.1, 0.2, 0.5, and 1 mg/L. The degradation reaction mixtures were transferred to a 37 °C water bath. A total of 2 μL mixed samples were collected at 15 min and 30 min to evaluate DNA fragment size changes via gel electrophoresis. Each collected sample was diluted to 10 μL by loading buffer (QSINGKE, Nanjing, China). Then, the diluted sample was quickly transferred to the loading holes in a 3% (w/v) agarose gel (after Gel-Red staining), which was placed in an electrophoresis tank containing 1× TAE buffer (Solarbio, Beijing, China). Meanwhile, 5 μL 80 ng/μL DL2000 DNA ladder solution (Takara, Dalian, China) was added to one hole (generally the first hole) of the agarose gel as a marker of gel electrophoresis progress. Gel electrophoresis was conducted at 6.0 V/cm. Then, the residual DNA fragments were imaged and visualized by a Molecular Imager FX equipped with Quantity One software (Bio-Rad, Hercules, Canada). Each experiment was repeated twice to confirm the reliability of the results. In addition, natural degradation of DNA (100 mg/L) in 30 min was evaluated under the same conditions without DNase I.

The absorbance change of DNA was measured to further clarify the facilitation mechanism of PFAAs on DNA degradation. Before adding the DNA degrading enzyme, the 99 μL reaction systems described above (including DNA, PFAAs, DNase I buffer, and Tris–HCl) were placed in a 96-well quartz plate, using the treatment without PFAAs as control. Then, the plate was placed into a Multi-Mode Microplate Reader (SpectraMax® iD5, Molecular Devices, USA) for detection. The relevant parameters (Time: 0, 15, 30 min; Absorbance: 260 nm) were set, and the absorbance of DNA was immediately detected at 37 °C after the addition of 1 μL DNase I (0.2 U/μL). The original data were translated to absorbance change (ΔA) values for DNA based on the DNA absorbance of the control. Thereafter, the curves describing the relationships between ΔA values and PFAA concentrations were fitted using OriginPro 2021 software to illustrate the effects of PFAA dose on DNA degradation.

2.2. Enzyme activity determination and AFM

DNase I enzyme activity was detected by the Multi-Mode Microplate Readers according to previous research, and the detailed procedures are shown in Supporting information [35]. Direct observation of DNA degradation can be achieved by AFM (Dimension® Icon™, Bruker, Germany), as reported previously [36]. The testing conditions are also shown in Supporting information.

2.3. Fluorescence titration experiments

To assess the PFAA–DNA binding interaction and PFAA–DNase I binding interaction, three-dimensional fluorescence titration tests were performed. For this purpose, a 2 mL Hoechst-probe-labeled DNA sample (10 mg/L) after PFAA titration (20 mg/L) or a 2 mL aliquot of mixed solution containing DNase I (6.25 mg/L) and PFAAs (0, 2.5, 5, 7.5, 10, 12.5, 15, 17.5, or 20 mg/L) was collected, and its fluorescence intensity was determined using a fluorescence spectrophotometer (F96PRO, Leng Guang, China). The excitation and emission wavelengths were set to 368 and 508 nm for the PFAA–DNA interaction and 286 and 355 nm for the PFAA–DNase I interaction (Supporting information S1).

2.4. Attenuated total reflection Fourier-transform infrared spectroscopy (ATR-FTIR) analysis

The intensity and position change of the stretching vibration peaks derived from specific functional groups of DNA or DNase I influenced by PFAAs can be used to explore the binding mechanism. DNA + PFAAs,

DNase I + PFAAs, and DNA + DNase I + PFAAs were analyzed using ATR-FTIR. Based on the DNA degradation experiments described above, we increased the concentrations of the reactants to obtain sufficient samples for ATR-FTIR measurement, i.e., 100 mg/L DNA, 50 mg/L DNase I, and 2 mg/L PFAAs. Detailed operating procedures and testing conditions are in Supporting information S1.

2.5. DNA molecular morphology analysis

UV–vis spectroscopy analysis was employed to assess the structural change of DNA after binding with PFAAs. For UV–vis analysis, 100 mg/L DNA and PFAAs (0, 0.5, and 1 mg/L) were obtained through dilution of their stock solutions (500 mg/L DNA and 200 mg/L PFAAs) using Tris–HCl (10 mmol/L, pH 7.4) solution. The mixed solutions were measured from 240 to 280 nm by a Spectrophotometer (UV-2600, Shimadzu, Kyoto, Japan) at room temperature after shaking for 30 min at 25 °C.

CD is an extremely sensitive analysis method frequently used to detect DNA conformation changes [37]. Thus, we performed CD measurements of DNA after binding with PFAAs to observe whether PFAA–DNA binding could induce DNA deformation (see Supporting information S1).

2.6. Density functional theory (DFT) calculation

We performed the DFT calculations using the dispersion-corrected meta-hybrid (ωB97XD) function in the Gaussian 16 program to investigate binding forces between DNA fragments and PFAAs. Based on the results of ATR-FTIR and fluorescence titration, AT base pairs in the DNA structure were the main site for PFAAs and DNA binding interactions. Considering that no digital model of salmon sperm DNA was currently available, the TTAA sequence, i.e., 5′-TpTp-3′ & 5′-ApAp-3′, was used as the alternative of salmon sperm DNA for DFT calculations in this study. This approach not only reflects the interaction between the AT base of DNA and pollutants but also simplifies the DFT calculations [38]. The 5′-TpTp-3′ & 5′-ApAp-3′ DNA was obtained by intercepting the TTAA sequence from the simple double-stranded DNA d(CGCGAATTCGCG)$_2$ (PDB ID: 2B0K) using Notepad++ software. Before intercepting the TTAA sequence, the unnecessary ligands in the DNA (PDB ID: 2B0K) were removed.

The mixture of 5′-TpTp-3′ & 5′-ApAp-3′ was combined individually with each PFAA (PFHxA, PFOA, PFNA, and PFOS) downloaded from http://www.chemspider.com/ using GaussView 5.0. Next, structural optimization and frequency analysis of each complex structure were conducted using Gaussian 16 with the ωB97XD/6–311+G** basis, which was selected for its relatively high accuracy and precision. Multiwfn_3.7 and VMD 1.9.3 program were used for the gradient isosurface of TTAA-PFAA and the reduced density gradient vs. electron density multiplied by the sign of the second Hessian eigenvalues [sign(λ_2)ρ] plots analysis. In addition, the latest independent gradient (IGM) theory [39] was introduced to assess weak intermolecular and intramolecular binding forces. Considering the possibility of complex halogen-bonding dispersion interactions occurring in the TTAA-PFAA binding interactions due to the C–F bonds in PFAA molecules, the analysis based on SAPT was used to perform energy decomposition calculation using the DFT calculation results and the PSI4 program [40,41]. SAPT analysis is considered a rigorous approach to quantitatively decompose the interactions between fragments based on energy, particularly the occurrence of halogen-bonding interactions [40,41].

2.7. Global ecological risk evaluation

To evaluate the global ecological risk levels of PFAAs, more than 90,000 data points distributed in global surface waters and groundwater were first collected. Based on the gel electrophoresis and DNA absorbance change tests, the ecological risk assessment criterion for evaluating the ecological risk of PFAAs was developed, i.e., PFAAs concentration < 0.02 mg/L for low ecological risk, the range of 0.02–0.5 mg/L for medium ecological risk, and > 0.5 mg/L for high ecological risk. The numbers of low, medium, and high ecological risk points were calculated by comparing the PFAAs concentration. ArcGIS Pro 2.8 software was used to mark the numbers and locations of different risk levels in various countries.

3. Results and discussion

3.1. PFAAs facilitate enzymatic degradation of DNA

It is reported that DNA can be degraded via hydrolysis, oxidation, and enzymatic reaction, while enzymatic reaction is considered the main degradation pathway in the natural environment [32]. Besides, according to previous studies, DNA enzymatic degradation can be affected by pollutants [25,26,32]. As shown in Fig. 1, the DNA fragments under control conditions without DNase I degradation (CK treatment) had molecular weights greater than 2,000 bp. These fragments exhibited a slight tailing phenomenon, as the concentration used here (100 mg/L) is generally characterized by a certain degree of natural degradation. After 15 min of degradation with DNase I, the DNA was degraded into small fragments with molecular weights ranging mainly from 100 bp to 1,500 bp. In the presence of PFAAs with concentrations > 0.02 mg/L, DNA was degraded by DNase I into fragments with molecular weights mainly below 1,000 bp, which were smaller than in the treatment without PFAAs. Furthermore, the degradation degree of DNA fragments was positively related to PFAA concentration. At PFAA ≥ 0.5 mg/L, DNA was degraded into fragments with molecular weights under 100 bp. Time was a favorable factor for DNA degradation, with the molecular weight of DNA degradation fractions decreasing to less than 200 bp after 30 min of degradation with DNase I. The gel electrophoresis experiments described above were repeated once (Fig. S1). The comparable data obtained from the two experiments confirmed the reliability of the gel electrophoresis results. These results indicate the promotion of the enzymatic degradation of DNA by PFAAs, even at low concentrations (0.02 and 0.05 mg/L). On the contrary, a previous study reported that phthalates inhibited the enzymatic degradation of DNA, because they could bind to amino groups in deoxyribonuclease I amino acid residues and lead to the alteration of the helix structure and structural deformation of deoxyribonuclease I [42]. These results indicated that the effects of organic pollutants on DNA degradation were pollutant-dependent.

As DNA degradation can cause exposure of its bases and thereby increase absorbance at 260 nm, the quantitative dose effects of PFAAs on DNA degradation were determined according to ΔA of DNA between degradation treatments with and without PFAAs. The results showed that ΔA values in the presence of PFAAs were significantly greater than 0 in all cases ($p < 0.05$, Fig. 2), indicating that PFAAs at the concentrations evaluated (0.02–1 mg/L) could markedly enhance DNA degradation. The ΔA values and PFAA concentrations conformed to significant S-shaped curves with $R^2 > 99\%$ ($p < 0.05$), regardless of the degradation reaction time (15 and 30 min) (Fig. 2), indicating a nonlinear dose effect of PFAAs on DNA degradation. Notably, ΔA values increased sharply with increasing PFAA concentrations at lower levels ($\leq$0.2 mg/L) but gently with PFAA concentrations exceeding 0.2 mg/L. These results are consistent with those obtained through gel electrophoresis experiments, further confirming that PFAAs can promote DNA degradation, even at low concentrations.

Interestingly, PFHxA, PFOA, and PFNA, which contain carboxyl groups, generally had stronger effects on DNA degradation than PFOS with a sulfonic acid group (Fig. S2). Significant differences ($p < 0.05$) were observed with 0.02, 0.2, 0.5, and 1 mg/L PFAAs at 15 min of DNA degradation and with 0.1, 0.2, and 0.5 mg/L of PFAAs at 30 min of DNA degradation (Fig. S2). This indicates that PFAAs with carboxyl groups are more conducive to DNA degradation than PFAAs with sulfonic acid groups, owing to stronger DNA binding effects of the former than the latter [43]. PFHxA, PFOA, and PFNA, with increasing carbon chain numbers, had comparable effects on DNA degradation, indicating that the carbon chains of the PFAAs had little influence on DNA degradation.

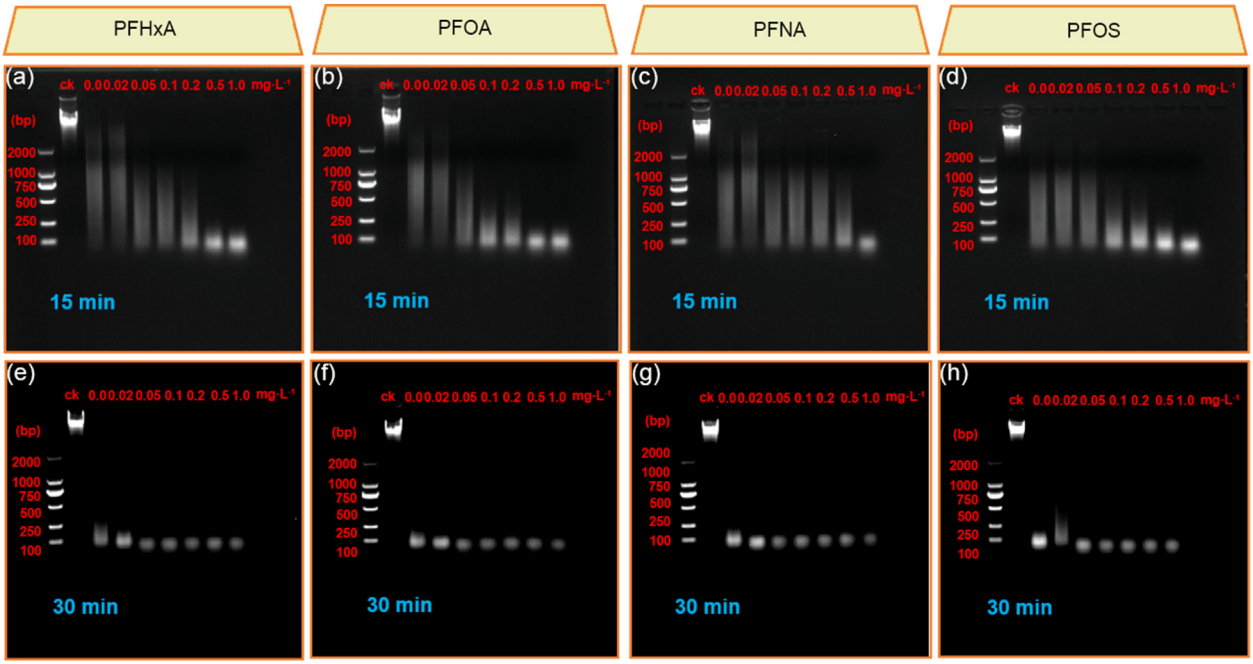

Fig. 1. Gel electrophoresis of DNA molecular fragments after enzymatic degradation with DNase I affected by (a, e) PFHxA, (b, f) PFOA, (c, g) PFNA, or (d, h) PFOS at 15 min and 30 min. CK was the control treatment, which included no DNase I. The PFAA concentrations were 0, 0.02, 0.05, 0.1, 0.2, 0.5, and 1.0 mg/L, respectively.

AFM images of DNA are presented in Figs. 3 and S3. DNA aggregation occurred at 100 mg/L. The edges of the DNA aggregates had a vague outline due to the uneven distribution of filamentous aggregates between the periphery and the central area (Fig. 3a). After degradation with DNase I, DNA molecules were altered from intact aggregates to irregular degradation products (Fig. 3b). The addition of PFAAs (e.g., PFOA) caused the edges of DNA aggregates to become brighter (Fig. 3c), indicating that PFAAs could bind to DNA. Compared to the molecular fragments of DNA obtained through DNase I degradation, the DNA fragments (Fig. 3d) treated with DNase I in the presence of DNA were significantly smaller. The AFM results of PFHxA–DNA, PFNA–DNA, and PFOS–DNA are consistent with those of PFOA–DNA fragments (Fig. S3). These indicate that PFAAs promote enzymatic degradation of DNA, consistent with the gel electrophoresis results described above.

3.2. Effects of PFAAs on natural DNA degradation

Three possible processes may have driven the promotion of DNA enzymatic degradation by PFAAs. First, the combination of PFAAs and DNA may promote the natural degradation of DNA. Second, PFAAs may bind to DNase I and thereby affect its degradation activity. Finally, PFAAs may bind to DNA and be inserted into its double helix molecular structure, leading to DNA deformation followed by degradation by DNase I [12–15]. These three possible processes must be tested individually. To explore whether PFAAs can cause natural degradation of DNA, gel electrophoresis was conducted using mixtures of DNA (100 mg/L) and each PFAA (0–1 mg/L) without DNase I. As shown in Fig. S4, the DNA fragments had nearly identical molecular weights greater than 2,000 bp and showed no apparent tailing. This indicates that PFAAs cause little natural degradation of DNA.

3.3. PFAAs influence the enzymatic activity of DNase I

In view of the results presented above, the effects of PFAAs on the activity of DNase I were explored. The increase of PFAA concentration from 0 to 1.0 mg/L led to almost no change in DNase I activity, which remained within 2.6 ± 0.10 Kunitz units for all PFAAs tested (Fig. S5). This illustrates that PFAAs cannot affect DNase I activity. Besides, FTIR spectra of DNase I revealed that PFAAs did not induce any functional group changes in DNase I (Fig. S6). This conclusion was reached because no shifts in characteristic peaks of DNase I were observed, including the peak at 1,647 cm^{-1} assigned to C═O or N═O stretching vibrations in amide I, the peaks at 1,541 and 1,456 cm^{-1} assigned to C–N and N–H, respectively, in amide II, and the peaks at 1,398 cm^{-1} and 1,242 cm^{-1} assigned to N–H bending and C–N stretching vibrations, respectively, in amide III. Therefore, this result confirms that PFAAs have no effect on DNase I activity.

To further evaluate whether PFAAs affect the enzymatic activity of DNase I, the interaction between DNase I and PFAAs was determined through fluorescence titration experiments (Fig. S7). As shown in Fig. S7a, the tested concentrations of PFAAs (0–20 mg/L) did not affect the maximum DNase I's fluorescence intensity at the optimal excitation (286 nm) and emission (355 nm) wavelength. No significant difference existed in the fluorescence of DNase I enzyme within 120 min in the presence of PFAAs at the highest dosage (20 mg/L). This finding ruled out the effects of PFAAs on the enzyme activity, because 120 min are generally sufficient for determining the interactions between DNase I enzyme and chemicals using fluorescence (Fig. S7b) [15]. This indicates that PFAAs cannot cause fluorescence quenching of DNase I, and thus cannot bind to DNase I and affect its degradation activity. Therefore, the promotion of DNA degradation by PFAAs was not related to DNase I activity.

3.4. PFAA–DNA binding and its influence on DNA deformation

As two possible mechanisms by which PFAAs may promote DNA degradation were excluded as described above, DNA deformation induced by PFAA binding was most likely responsible for the promotion effect. Here, PFAA–DNA binding was tested through Hoechst-labeled DNA fluorescence quenching reactions in the presence of PFAAs. Apparent fluorescence quenching of DNA was observed, which conformed to the Stern–Volmer equation ($R^2 > 0.93$, Fig. S8 and Table S1), suggesting a dynamic quenching process induced by PFAA binding.

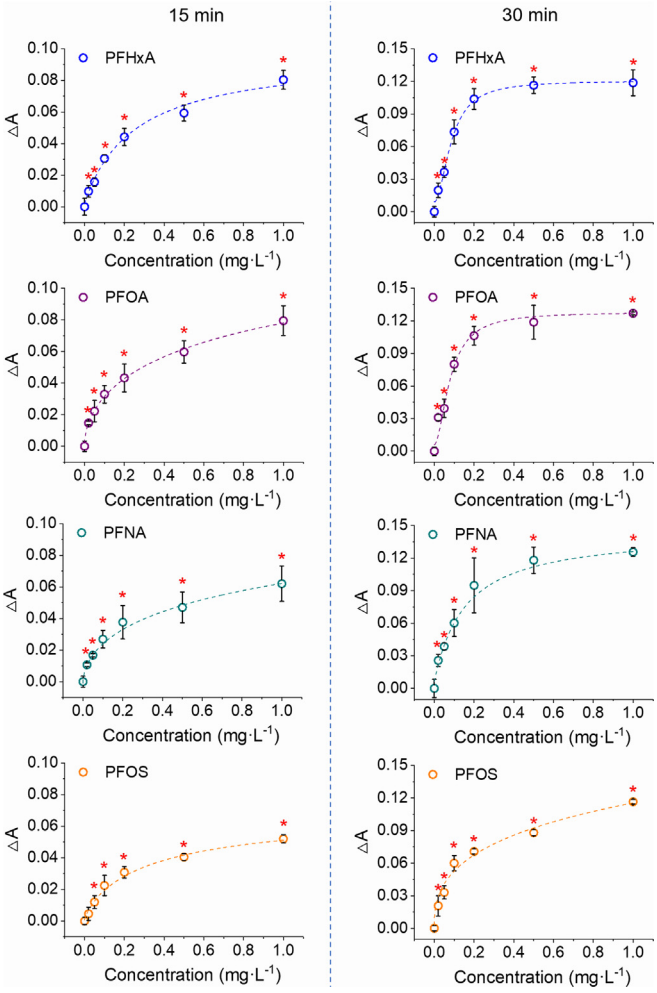

Fig. 2. DNA absorbance increases driven by four typical perfluoroalkyl acids at 15 min and 30 min of DNA enzymatic degradation. * indicates that ΔA in the presence of PFAAs at all tested concentrations (0.02–1 mg/L) was significantly greater than 0 (i.e., the treatment without PFAAs).

Hoechst is a cell-permeable benzimidazole dye that binds to the minor groove of double-stranded DNA, preferentially binding to AT base pairs. Thus, this result also confirmed that AT base pairs in the DNA structure were the main site for PFAAs and DNA binding interactions. Such a binding site could be associated with the structure compatibility between the PFAAs and AT base pairs of DNA. The quenching constants (K_{SV}) for PFHxA, PFOA, PFNA, and PFOS binding with DNA were calculated to be 2.47×10^5, 2.40×10^5, 2.91×10^5, and 3.00×10^5 L/mol, respectively. This demonstrates that PFAAs with carboxyl groups bind DNA more readily than PFAAs with sulfonic acid groups, while the carbon chain length has little effect on PFAA binding to DNA. The K_q values for PFHxA, PFOA, PFNA, and PFOS binding with DNA were estimated to be $(0.21–1.83) \times 10^{13}$, $(0.19–1.60) \times 10^{13}$, $(0.23–1.94) \times 10^{13}$, and $(0.23–2.00) \times 10^{13}$ L/(mol·s), which were 2–3 orders of magnitude than the maximum K_q value [2.00×10^{10} L/(mol·s)] of a biopolymer. This result suggested the co-occurrence of a static quenching process [44]. Accordingly, the fluorescence quenching data were fitted to a static quenching equation (in Supporting information S1), resulting in $R^2 > 0.96$. The static binding constants (K_A) of PFAA–DNA were calculated as 203.24, 353.18, 2,518.26, and 688.18 L/mol with corresponding n values of 0.49, 0.55, 0.68, 0.58 for PFHxA, PFOA, PFNA, PFOS, respectively. These fluorescence quenching results confirm that a binding interaction occurs between PFAAs and DNA.

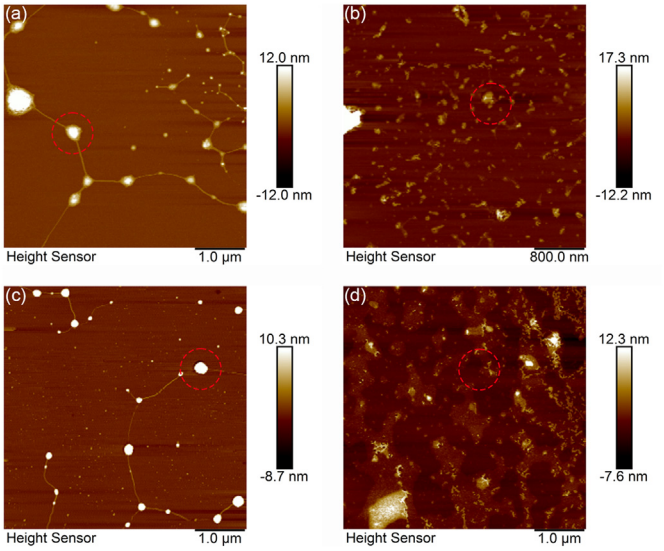

Fig. 3. Trapping-mode AFM topographical images of (a) free salmon sperm DNA, (b) DNA degraded with DNase I, (c) PFOA-DNA, and (d) DNA degraded by DNase I in the presence of PFOA. The concentrations for DNA and PFOA were set to 100 mg/L and 1.0 mg/L, respectively. The red circle in the figures indicates DNA or its fragments.

To exclude the interference effects of PFAAs on the Hoechst fluorescence spectra, we compared the fluorescence spectra of Hoechst (5 mg/L) with and without the addition of the target PFAAs (0–26.64 μg/L). Little change was observed in the intensity and position of the fluorescence peak of Hoechst in the presence of PFAAs (Figs. S9 and S10). This indicated that PFAAs could not bind with Hoechst and thereby cause fluorescence quenching. Next, a typical intercalation probe (acridine orange) was used to detect the possibility of intercalation during the PFAAs–DNA binding interaction. The results showed that PFAAs could not induce any fluorescence quenching of acridine orange-labeled DNA, which indicated that PFAAs–DNA binding was not in an intercalative manner (Fig. S11). Therefore, we excluded the contribution of intercalation on the binding interaction of PFAAs and DNA.

PFAA–DNA binding may induce DNA deformation, which would likely enhance the enzymatic degradation of DNA. Such DNA deformation can generally be studied using CD [45]. Generally, the CD of a common B-configuration DNA contains a negative peak at about 248 nm and a positive peak at about 278 nm [37], reflecting the right-handed helicity and base stacking of DNA, respectively. With the addition of PFHxA (0–31.65 μmol/L), PFOA (0–24.15 μmol/L), PFNA (0–21.65 μmol/L), or PFOS (0–24.00 μmol/L), the intensity of DNA CD spectra at both the positive (278 nm) and negative (248 nm) peaks decreased significantly, with no shift of the peak position (Fig. 4a). This demonstrates that PFAA binding to DNA induces decreases in right-handed helicity and base stacking in the DNA structure, loosening the DNA molecular structure. This change in DNA structure supported access to more digestion sites for DNase I, thereby promoting the enzymatic degradation of DNA.

3.5. PFAA–DNA binding sites and mechanisms

Fig. 4b illustrates the ATR-FTIR spectral characteristics of DNA, as well as the combinations of PFAA–DNA and PFAA–DNase I–DNA. Generally, the spectral range at 600–1,800 cm^{-1} represents the asymmetric and symmetric stretching vibration peaks of nitrogenous bases, phosphate, and deoxyribose in the DNA structure [46]. Specifically, the C═O or C═N stretching vibrations of guanine (G), thymine (T), adenine (A), and cytosine (C) were, respectively, at 1,693, 1,659, 1,608, and

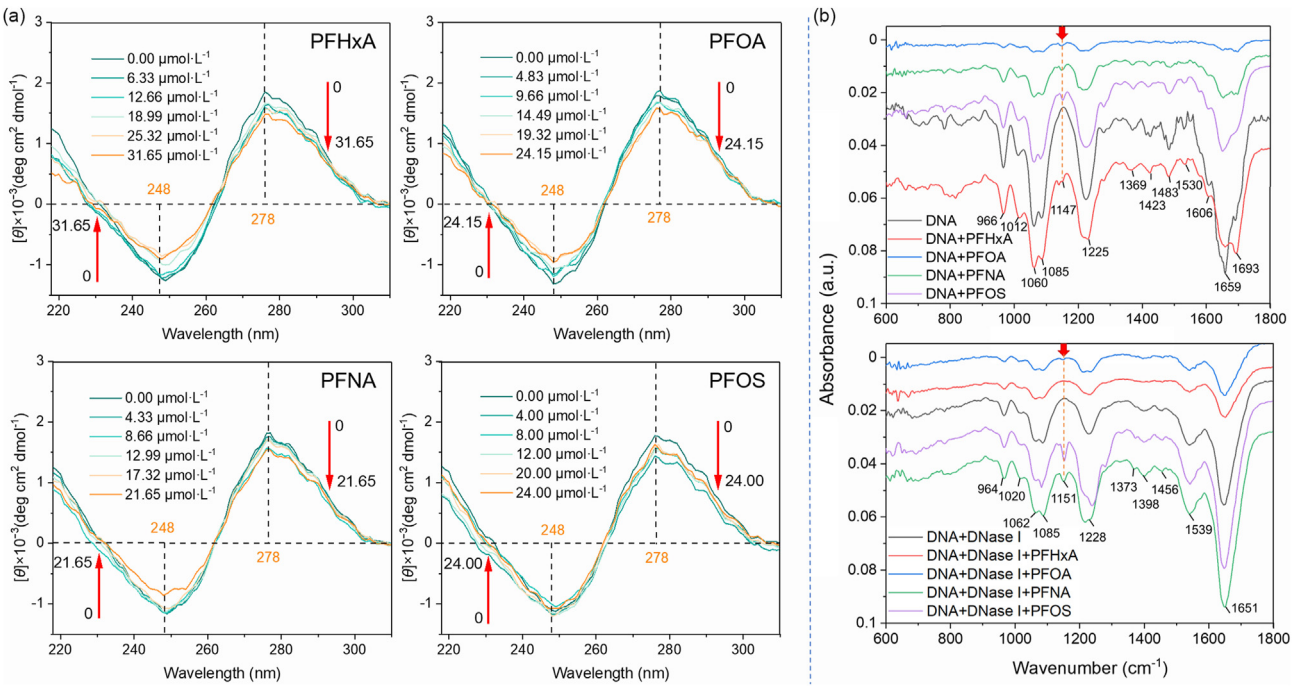

Fig. 4. Circular dichroism spectra (a) of DNA after binding with various concentrations of PFHxA (0–31.65 μmol/L), PFOA (0–24.15 μmol/L), PFNA (0–21.65 μmol/L), or PFOS (0–24.00 μmol/L) and FTIR spectra (b) of DNA and DNA–DNase I binding with and without PFHxA, PFOA, PFNA, and PFOS. Red arrows indicate the main changes in spectral peaks.

1,483 cm^{-1} of DNA. The vibrational band at 1,225 cm^{-1} was assigned to the B-conformation of DNA. Vibrational bands at 1060 and 1085 cm^{-1} reflected the asymmetric stretching vibration of phosphate, while those at 966 cm^{-1} reflected the symmetric stretching vibration of phosphate (Fig. 4b) [46]. In the presence of PFAAs, the thymine band of DNA shifted from 1,658 to 1,660, 1,652, 1,652, and 1,651 cm^{-1}, respectively. However, there was no significant band shift of guanine, adenine, cytosine, phosphate vibrations, or the B-conformation of DNA. Interestingly, a new peak assigned to the C–F stretching vibration at 1,147 cm^{-1} was observed after binding with PFHxA, PFOA, PFNA, and PFOS, which further confirmed the PFAAs–DNA binding interaction (Fig. 4b). These results indicate that chain-like PFAA molecules could be inserted into the B-DNA structure and undergo binding interaction, with the most probable binding sites being regions of B-DNA that are rich in AT base pairs. In the presence of DNA, DNase I, and PFAAs, the thymine peak shift caused by the binding of PFAAs to DNA was not affected, although DNase I concealed some DNA functional groups, e.g., the peak at 1,693 cm^{-1} disappeared (Fig. 4b). This indicates that DNase I does not affect DNA–PFAA binding, and that conversely, such binding may be beneficial to DNA degradation by DNase I due to loosening of the DNA structure.

The binding of organic pollutants with DNA occurs mainly in the noncovalent binding mode, driven by weak interactions such as van der Waals forces, hydrophobic interactions, hydrogen bonds, and electrostatic interactions. Noncovalent binding of organic pollutants to DNA can be divided into three specific modes: intercalation, groove binding, and electrostatic interaction [47]. UV–vis spectroscopy is commonly used to explore the binding mode between organic pollutants and DNA [47,48]. When organic pollutants bind to DNA via intercalation, they expose more DNA bases, leading to increased absorbance by DNA and a hyperchromic effect [48]. By contrast, groove binding can be identified based on a hypochromic effect accompanied by no or a minor red shift in the UV–vis peak of DNA [49]. Fig. S12 displays the UV–vis spectra of DNA after binding with PFAAs. The characteristic peak at 260 nm assigned to the π–π* transition of DNA base pairs was clearly observed. The DNA absorbance at 260 nm decreased with the PFAAs concentrations increased from 0 to 1 mg/L. This result indicated that the PFAA–DNA binding interaction was in groove binding mode. As Hoechst is a non-intercalating fluorescent dye, the quenching of Hoechst-labeled DNA caused by PFAAs further supported that DNA–PFAA binding was groove binding rather than intercalation (Fig. S8).

Weak interaction forces play an important role in gene regulation, including transcription, replication, and other biological processes at the molecular level [50]. At the same time, these forces are critical to regulating the functions of biological macromolecules [51]. DFT calculations [52] were conducted to clarify the weak interaction forces involved in the binding interaction between PFAA and DNA. The formation of plump green flakes in the interaction between PFAAs and 5′-TpTp-3′ & 5′-ApAp-3′ molecules (Fig. 5), indicated by orange arrows, illustrates the van der Waals forces between PFAAs and 5′-TpTp-3′ & 5′-ApAp-3′ molecules. Moreover, small blue circle parts on top of the plump green flakes suggest the formation of hydrogen bonds during DNA–PFAA binding interactions. In addition, $\delta g^{inter/intra}$ vs. sign(λ_2)ρ scatter plots were presented to further quantify the intermolecular interaction between PFAAs and 5′-TpTp-3′ & 5′-ApAp-3′ molecules. The large number of black points at sign(λ_2)ρ > 0 indicates a repulsive force between each PFAA and 5′-TpTp-3′ & 5′-ApAp-3′ molecules. The appearance of a small $\delta g^{inter/intra}$ peak at −0.04 suggests the formation of hydrogen bonds during DNA–PFAA binding interactions. In addition, numerous points were present in the range of sign(λ_2)ρ < −0.04, demonstrating that van der Waals forces. Thus, van der Waals forces and hydrogen bonds were major binding forces.

Furthermore, the binding energies (Δ*E*), SAPT interaction energies, and related parameters of DNA (TTAA base)–PFAA interactions were analyzed based on the results of quantum chemistry calculations (Tables S2–S4). The binding energies of TTAA–PFHxA, TTAA–PFOA, TTAA–PFNA, and TTAA–PFOS calculated using the equation ($\Delta E = E_{TTAA\text{-}PFAAs} - E_{TTAA} - E_{PFAAs}$) were −1.090, −1.118, −1.137, and

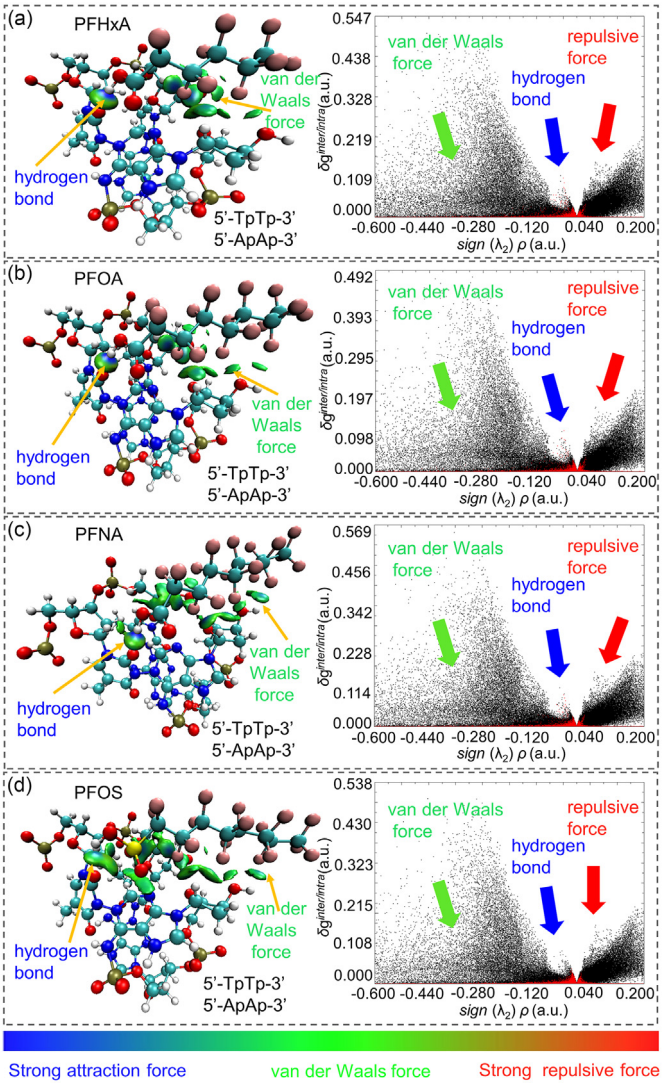

Fig. 5. Gradient isosurface of the main section for complexes of 5′-TpTp-3′ & 5′-ApAp-3′ with PFHxA (a), PFOA (b), PFNA (c), and PFOS (d), and plots of the reduced density gradient ($\delta g^{inter/intra}$) vs. sign(λ_2)ρ. The surfaces are colored on a blue-green-red scale according to the magnitude and sign(λ_2)ρ value, ranging from −0.6 to +0.2 a.u. The blue, green, and red colors indicate strong attractive interactions, very weak interactions, and strong repulsive non-bonding overlap, respectively. N, H, C, O, and F atoms are shown as blue, white, cyan, red, and pink spheres, respectively.

−1.257 eV, respectively (Table S2). These consistently negative binding energies indicate that the binding interaction between TTAA and PFAAs is an exothermic reaction; thus, the overall energy is reduced to get a more stable state. SAPT analysis results (Table S3) showed that the total interaction energy between DNA (TTAA bases) and PFHxA was −76.634 kJ/mol, in which the electrostatic, exchange, induction, and dispersion effects contributed −76.881, 134.365, −33.382, and −100.286 kJ/mol, respectively. Thus, the main contributor to the TTAA–PFHxA binding interaction regarding van der Waals forces was the dispersion force, while electrostatic and induction effects were relatively minor but not completely negligible. The same general result was observed for PFOA, PFNA, and PFOS. The carbon chains appeared to have minor effects on interaction energy, as comparable values were obtained for all perfluorocarboxylic acids tested. Interestingly, sulfonic acid-substituted PFOS (−106.182 kJ/mol) had lower interaction energy than carboxyl-substituted PFHxA (−76.634 kJ/mol), PFOA (−72.919 kJ/mol), and PFNA (−77.697 kJ/mol). This result might be attributed to PFOS having lower dipole moment, electron affinity, and electrophilicity values than that of other PFAAs (Table S4). The effects of PFAA physicochemical properties on DNA binding were generally consistent with those on DNA degradation (Figs. 1 and 2), confirming that PFAAs could facilitate DNA degradation through binding interactions.

Compared to previous studies regarding DNA degradation driven by organic pollutants (mainly those with benzene rings or benzene-like rings), this study reported the dose-dependent effects and mechanisms of the typically chain-like ionic organic pollutants (PFAAs) on enzymatic DNA degradation for the first time. This study also quantitatively described the contributions of van der Waals force to the PFAAs–DNA binding using SAPT analysis, clarifying the important role of dispersion force in PFAAs–DNA binding. The findings of this study showed that PFAAs could decrease base stacking and right-handed helicity of DNA by binding to AT bases in a groove-binding mode via dispersion force and hydrogen bonding, thus promoting DNA degradation. Such a DNA degradation mechanism was quite different from those in the previous reports, which gave insight into the DNA degradation driven by organic pollutants, highlighting the significance of this study (Table S5).

3.6. Global ecological risk of PFAAs

The fragment sizes after DNA degradation without addition of PFAAs were the same with those added with 0.02 mg/L PFAAs, indicating that 0.02 mg/L PFAAs had no effect on DNA degradation (Fig. 1). When the concentration of PFAAs was more than 0.02 mg/L, the degradation fragments of DNA started to be smaller than the control (without PFAAs), indicating that ≥0.02 mg/L PFAAs could induce DNA degradation. Interestingly, the reduction in DNA degradation fragments was obviously greater when the concentration of PFAAs was more than 0.5 mg/L, indicating that ≥0.5 mg/L PFAAs strongly facilitated DNA degradation. Besides, another work reporting the effects of chlorpyrifos and chlorpyrifos-methyl facilitated DNA degradation also confirmed that 0.02 mg/L and 0.5 mg/L were two thresholds that cause DNA degradation and strongly promoted DNA degradation, respectively [25]. Accordingly, a crude criterion for evaluating the molecular ecological risk of PFAAs based on their concentration and resultant DNA degradation was developed, i.e., low molecular ecological risk (<0.02 mg/L PFAAs), medium molecular ecological risk (0.02–0.5 mg/L PFAAs), and high molecular ecological risk (>0.5 mg/L PFAAs). Using the above ecological risk assessment criterion, we analyzed the risk levels of PFAAs at 93,815 collected data points distributed in global surface waters and groundwater [53]. The results showed that the PFAA contamination in 527 points showed medium and high molecular ecological risk, although such contamination in all the other points presented a low molecular ecological risk. To be specific, 30 samples in USA (17), Canada (9), and China (4) were of high ecological risk; and 497 samples in USA (355), China (95), Canada (17), Australia (4), Czech Republic (3), Germany (1), Japan (4), Malaysia (11), Spain (1), and Sweden (6) were of medium ecological risk (Fig. 6 and Fig. S13). The results presented the potential ecological risk of PFAA contamination and warranted further and in-depth studies on the ecological risks of PFAA contamination, especially in highly contaminated areas, such as the USA, Canada, and China. These results can provide a reference for the research methodology of other emerging pollutants, since eDNA degradation is considered an important method for evaluating the effects of chemical contamination [19]. Considering the dose effects of the pollutants on the DNA degradation varied among their structures and properties, the criterion of the ecological risk based on the DNA degradation should be pollutant-dependent.

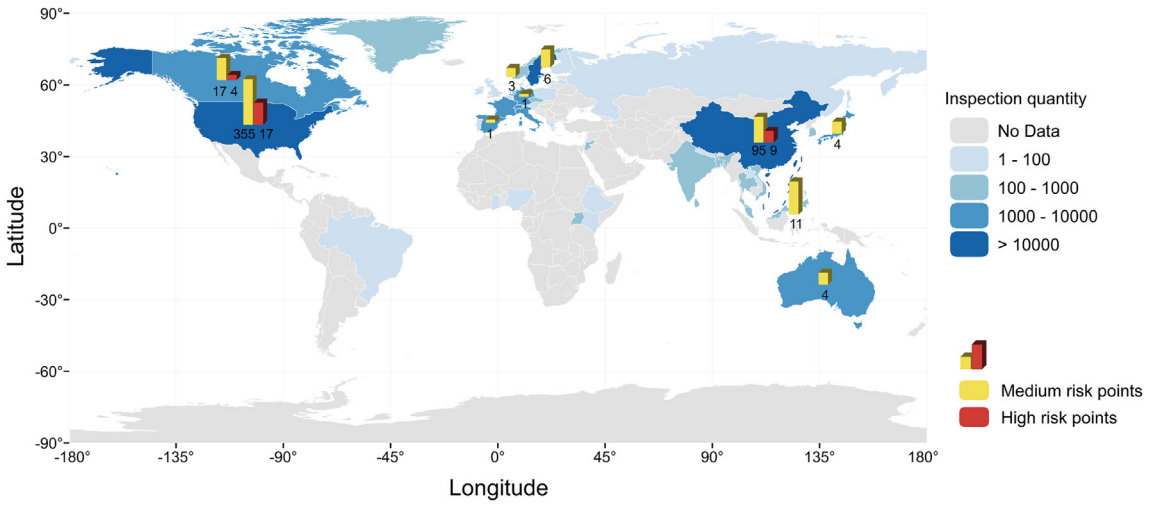

Fig. 6. Global ecological risk of PFAAs distributed in global surface waters and groundwater. The blue-filled sections of the world map indicate the inspection quantity for each country. Yellow and red represent the number of medium and high-risk points, respectively.

4. Conclusions

The findings from this work confirm that eDNA degradation is facilitated by PFAA binding. Such binding happens between PFAAs and DNA rather than between PFAAs and DNase I (protein), despite PFAAs being considered proteophilic compounds. PFAAs can bind to sequences rich in AT base pairs in the minor groove of eDNA through van der Waals forces (particularly dispersion force) and hydrogen bonds. Such binding can lead to reductions in eDNA base stacking and right-handed helicity, exposing more interaction sites to degrading enzymes and thereby enhancing DNA degradation. The global ecological risk evaluation results indicated that PFAA contamination could cause medium and high molecular ecological risk in some highly contaminated countries, such as the USA, Canada, and China, highlighting the significance of PFAA–DNA binding and its profound molecular ecological effects.

Author contributions

C.Q.: investigation, conceptualization, writing–original draft. R.-H.Z., X.J.H.: visualization, methodology. Z.K.L., H.-M.Z.: methodology. Y.-W.L.: validation, writing–review. N.-X.F., H.L., Q.-Y.C., Y.Z.G.: writing–review. L.X.: conceptualization, supervision, validation. C.-H.M.: conceptualization, funding acquisition, project administration. B.S.X.: writing–review & editing.

Declaration of competing interests

The authors declare no conflicts of interest.

Acknowledgments

This work was funded by the National Natural Science Foundation of China (42030713, 42107221, 42177187), Fundamental Research Funds for the Cornell University (21622109), and the Natural Science Foundation of Guangdong Province (2020A1515110535, 2018A030310629).

Appendix A. Supplementary data

Supplementary data to this article can be found online at https://doi.org/10.1016/j.eehl.2023.09.002.

References

[1] W. An, L. Duan, Y. Zhang, B. Wang, C.S. Liu, Occurrence, spatiotemporal distribution, seasonal and annual variation, and source apportionment of poly- and perfluoroalkyl substances (PFASs) in the northwest of Tai Lake Basin, China, J. Hazard. Mater. 416 (2021) 125784, https://doi.org/10.1016/j.jhazmat.2021.125784.

[2] H. Mahoney, Y. Xie, M. Brinkmann, J.P. Giesy, Next generation per-and poly-fluoroalkyl substances: status and trends, aquatic toxicity, and risk assessment, Eco-Environ. Health 1 (2) (2022) 117–131, https://doi.org/10.1016/j.eehl.2022.05.002.

[3] L. Xie, X. Wang, X. Dong, L. Su, H. Zhu, C. Wang, et al., Concentration, spatial distribution, and health risk assessment of PFASs in serum of teenagers, tap water and soil near a Chinese fluorochemical industrial plant, Environ. Int. 146 (2021) 106166, https://doi.org/10.1016/j.envint.2020.106166.

[4] X. Yao, L. Zhong, Genotoxic risk and oxidative DNA damage in HepG2 cells exposed to perfluorooctanoic acid, Mut. Res. 587 (1) (2005) 38–44, https://doi.org/10.1016/j.mrgentox.2005.07.010.

[5] G. Leter, C. Consales, P. Eleuteri, R. Uccelli, I.O. Specht, G. Toft, et al., Exposure to perfluoroalkyl substances and sperm DNA global methylation in Arctic and European populations, Environ. Mol. Mutagen. 55 (7) (2014) 591–600, https://doi.org/10.1002/em.21874.

[6] G. Liu, S. Zhang, K. Yang, L. Zhu, D. Lin, Toxicity of perfluorooctane sulfonate and perfluorooctanoic acid to *Escherichia coli*: membrane disruption, oxidative stress, and DNA damage induced cell inactivation and/or death, Environ. Pollut. 214 (2016) 806–815, https://doi.org/10.1016/j.envpol.2016.04.089.

[7] C. Liu, V.W. Chang, K.Y. Gin, V.T. Nguyen, Genotoxicity of perfluorinated chemicals (PFCs) to the green mussel (*Perna viridis*), Sci. Total Environ. 487 (2014) 117–122, https://doi.org/10.1016/j.scitotenv.2014.04.017.

[8] I. Nobels, F. Dardenne, W.D. Coen, R. Blust, Application of a multiple endpoint bacterial reporter assay to evaluate toxicological relevant endpoints of perfluorinated compounds with different functional groups and varying chain length, Toxicol. In Vitr. 24 (6) (2010) 1768–1774, https://doi.org/10.1016/j.tiv.2010.07.002.

[9] F. Coperchini, L. Croce, M. Denegri, P. Pignatti, M. Agozzino, G.S. Netti, et al., Adverse effects of in vitro GenX exposure on rat thyroid cell viability, DNA integrity and thyroid-related genes expression, Environ. Pollut. 264 (2020) 114778, https://doi.org/10.1016/j.envpol.2020.114778.

[10] X. Zhang, L. Chen, X. Fei, Y. Ma, H. Gao, Binding of PFOS to serum albumin and DNA: insight into the molecular toxicity of perfluorochemicals, BMC Mol. Biol. 10 (1) (2009) 16, https://doi.org/10.1186/1471-2199-10-16.

[11] M. Nagler, H. Insam, G. Pietramellara, J. Ascher-Jenull, Extracellular DNA in natural environments: features, relevance and applications, Appl. Microbiol. Biot. 102 (15) (2018) 6343–6356, https://doi.org/10.1007/s00253-018-9120-4.

[12] K. Wasmund, C. Pelikan, A. Schintlmeister, M. Wagner, M. Watzka, A. Richter, et al., Genomic insights into diverse bacterial taxa that degrade extracellular DNA in marine sediments, Nat. Microbiol. 6 (2021) 885–898, https://doi.org/10.1038/s41564-021-00917-9.

[13] M. Chambard, C. Plasson, C. Derambure, S. Coutant, I. Tournier, B. Lefranc, et al., New insights into plant extracellular DNA. A study in soybean root extracellular trap, Cells 10 (1) (2021) 69, https://doi.org/10.3390/cells10010069.

[14] A.L. Hynen, J.J. Lazenby, G.M. Savva, L.C. McCaughey, L. Turnbull, L.M. Nolan, et al., Multiple holins contribute to extracellular DNA release in *Pseudomonas aeruginosa* biofilms, Microbiology 167 (2) (2021) 990, https://doi.org/10.1099/mic.0.000990.

[15] S.I. Pathan, P. Arfaioli, M.T. Ceccherini, J. Ascher-Jenull, P. Nannipieri, G. Pietramellara, et al., Physical protection of extracellular and intracellular DNA in soil aggregates against simulated natural oxidative processes, Appl. Soil Ecol. 165 (2021) 104002, https://doi.org/10.1016/j.apsoil.2021.104002.

[16] I.L. Brito, Examining horizontal gene transfer in microbial communities, Nat. Rev. Microbiol. 19 (7) (2021) 442–453, https://doi.org/10.1038/s41579-021-00534-7.

[17] M. Liu, A. Hata, H. Katayama, I. Kasuga, Consecutive ultrafiltration and silica adsorption for recovery of extracellular antibiotic resistance genes from an urban river, Environ. Pollut. 260 (2020) 114062, https://doi.org/10.1016/j.envpol.2020.114062.
[18] D. Calderón-Franco, M.C.M. van Loosdrecht, T. Abeel, D.G. Weissbrodt, Free-floating extracellular DNA: systematic profiling of mobile genetic elements and antibiotic resistance from wastewater, Water Res. 189 (2021) 116592, https://doi.org/10.1016/j.watres.2020.116592.
[19] P. Wang, Z. Yan, S. Yang, S. Wang, X. Zheng, J. Fan, et al., Environmental DNA: an emerging tool in ecological assessment, Bull. Environ. Contam. Toxicol. 103 (5) (2019) 651–656, https://doi.org/10.1007/s00128-019-02720-z.
[20] K. Kagzi, R.M. Hechler, G.F. Fussmann, M.E. Cristescu, Environmental RNA degrades more rapidly than environmental DNA across a broad range of pH conditions, Mol. Ecol. Resour. 22 (7) (2022) 2640–2650, https://doi.org/10.1111/1755-0998.13655.
[21] A. Nicholson, D. McIsaac, C. MacDonald, P. Gec, B.E. Mason, W. Rein, et al., An analysis of metadata reporting in freshwater environmental DNA research calls for the development of best practice guidelines, Environ. DNA 2 (3) (2020) 343–349, https://doi.org/10.1002/edn3.81.
[22] A.P. Popov, A.S. Konichev, I.L. Tsvetkov, Effect of toxic industrial pollutants on the activity and isoforms of acid DNase in the freshwater snail *Viviparus viviparusL*, Appl. Biochem. Microbiol. 39 (5) (2003) 454–458, https://doi.org/10.1023/A:1025436400412.
[23] F. Kang, Y. Gao, Q. Wang, Inhibition of free DNA degradation by the deformation of DNA exposed to trace polycyclic aromatic hydrocarbon contaminants, Environ. Sci. Technol. 44 (23) (2010) 8891–8896, https://doi.org/10.1021/es103215b.
[24] M. Woegerbauer, H. Burgmann, J. Davies, W. Graninger, DNase I induced DNA degradation is inhibited by neomycin, J. Antibiot. 53 (3) (2000) 276–285, https://doi.org/10.7164/antibiotics.53.276.
[25] B. Yang, C. Qin, X. Hu, K. Xia, C. Lu, F.O. Gudda, et al., Enzymatic degradation of extracellular DNA exposed to chlorpyrifos and chlorpyrifos-methyl in an aqueous system, Environ. Int. 132 (2019) 105087, https://doi.org/10.1016/j.envint.2019.105087.
[26] C. Qin, B. Yang, W. Zhang, W. Ling, C. Liu, J. Liu, et al., Organochlorinated pesticides expedite the enzymatic degradation of DNA, Commun. Biol. 2 (1) (2019) 1–9, https://doi.org/10.1038/s42003-019-0326-5.
[27] R. Elshafey, G.F. Abo-Sobehy, A. Radi, Graphene oxide/graphene quantum dots: a platform for probing ds-DNA-dimethoate interaction and dimethoate sensing, J. Electroanal. Chem. 899 (3) (2021) 115678, https://doi.org/10.1016/j.jelechem.2021.115678.
[28] K. Morawska, W. Ciesielski, S. Smarzewska, First electroanalytical studies of methoxyfenozide and its interactions with dsDNA, J. Electroanal. Chem. 882 (2021) 115030, https://doi.org/10.1016/j.jelechem.2021.115030.
[29] P. Cai, Q. Huang, X. Zhang, H. Chen, Adsorption of DNA on clay minerals and various colloidal particles from an Alfisol, Soil Biol. Biochem. 38 (3) (2006) 471–476, https://doi.org/10.1016/j.soilbio.2005.05.019.
[30] P. Cai, Q. Huang, X. Zhang, Interactions of DNA with clay minerals and soil colloidal particles and protection against degradation by DNase, Environ. Sci. Technol. 40 (9) (2006) 2971–2976, https://doi.org/10.1021/es0522985.
[31] C. Qin, F. Kang, W. Zhang, W. Shou, X. Hu, Y. Gao, Environmentally-relevant concentrations of Al(III) and Fe(III) cations induce aggregation of free DNA by complexation with phosphate group, Water Res. 123 (2017) 58–66, https://doi.org/10.1016/j.watres.2017.06.043.
[32] C. Qin, B. Yang, H. Cheng, X. Hu, Y. Gao, Non-covalent binding interaction and mechanism between polycyclic aromatic hydrocarbons and extracellular DNA, Chin. Sci. Bull. 67 (2022) 74–84, https://doi.org/10.1360/TB-2021-0927 (in Chinese).
[33] M.P. Rodero, A. Tesser, E. Bartok, I.R. Gillian, D.M. Erika, D. Marine, et al., Type I interferon-mediated autoinflammation due to DNase II deficiency, Nat. Commun. 8 (2017) 2176, https://doi.org/10.1038/s41467-017-01932-3.
[34] M. Engavale, J. McCord, B. Mapp, N. Nzimulinda, E. Bengtson, R.B. Sutton, et al., Dnase1 family in autoimmunity, Encyclopedia 1 (3) (2021) 527–541, https://doi.org/10.3390/encyclopedia1030044.
[35] T. Yasuda, S. Awazu, W. Sato, R. Iida, Y. Tanaka, K. Kishi, Human genetically polymorphic deoxyribonuclease: purification, characterization, and multiplicity of urine deoxyribonuclease I, J. Biochem. 108 (3) (1990) 393–398, https://doi.org/10.1093/oxfordjournals.jbchem.a123212.
[36] S. Ramakrishnan, B. Shen, M.A. Kostiainen, G. Grundmeier, A. Keller, V. Linko, Real-time observation of superstructure-dependent DNA origami digestion by DNase I using high-speed atomic force microscopy, Chembiochem 20 (22) (2019) 2818–2823, https://doi.org/10.1002/cbic.201900369.
[37] J. Kypr, I. Kejnovská, D. Renčiuk, M. Vorlíčková, Circular dichroism and conformational polymorphism of DNA, Nucleic Acids Res. 37 (6) (2009) 1713–1725, https://doi.org/10.1093/nar/gkp026.
[38] C.S. Hines, C. Meghoo, S. Shetty, M. Biburger, M. Brenowitz, R.S. Hegde, DNA structure and flexibility in the sequence-specific binding of papillomavirus E2 proteins, J. Mol. Biol. 276 (4) (1998) 809–818, https://doi.org/10.1006/jmbi.1997.1578.
[39] C. Lefebvre, H. Khartabil, J. Boisson, J. Contreras-García, J. Piquemal, E. Hénon, The independent gradient model: a new approach for probing strong and weak interactions in molecules from wave function calculations, ChemPhysChem 19 (6) (2018) 724–735, https://doi.org/10.1002/cphc.201701325.
[40] L.N. Anderson, F.W. Aquino, A.E. Raeber, X. Chen, B.M. Wong, Halogen bonding interactions: revised benchmarks and a new assessment of exchange vs dispersion, J. Chem. Theory Comput. 14 (1) (2018) 180–190, https://doi.org/10.1021/acs.jctc.7b01078.
[41] K.E. Riley, P. Hobza, Investigations into the nature of halogen bonding including symmetry adapted perturbation theory analyses, J. Chem. Theory Comput. 4 (2) (2008) 232–242, https://doi.org/10.1021/ct700216w.
[42] C. Qin, H. Cheng, B. Yang, Y. Xu, X. Hu, Y. Gao, et al., Binding of phthalates with nuclease increases DNA enzymatic degradation and implication for antibiotic resistance, Environ. Chem. Lett. 21 (2023) 31–39, https://doi.org/10.1007/s10311-022-01517-7.
[43] C. Qin, Y.X. Lu, T. Borch, L.L. Yang, Y.W. Li, H.M. Zhao, et al., Interactions between extracellular DNA and perfluoroalkyl acids (PFAAs) decrease the bioavailability of PFAAs in Pakchoi (*Brassica chinensis* L.), J. Agric. Food Chem. 70 (46) (2022) 14622–14632, https://doi.org/10.1021/acs.jafc.2c04597.
[44] J.R. Lakowicz, Principles of Fluorescence Spectroscopy, Springer Science & Business Media, Berlin, 2013.
[45] R. Lyng, T. Härd, B. Norden, Induced CD of DNA intercalators: electric dipole allowed transitions, Biopolymers 26 (8) (1987) 1327–1345, https://doi.org/10.1002/bip.360260809.
[46] G. Magdy, F. Belal, A.F. Abdel Hakiem, A.M. Abdel-Megied, Salmon sperm DNA binding study to cabozantinib, a tyrosine kinase inhibitor: multi-spectroscopic and molecular docking approaches, Int. J. Biol. Macromol. 182 (2021) 1852–1862, https://doi.org/10.1016/j.ijbiomac.2021.05.164.
[47] S. Kou, K. Zhou, Z. Lin, Y. Lou, J. Shi, Y. Liu, Insights into the binding properties of calf thymus DNA with lopinavir from spectroscopic and computational studies, J. Mol. Liq. 328 (2021) 115491, https://doi.org/10.1016/j.molliq.2021.115491.
[48] J. Shi, K. Zhou, Y. Lou, D. Pan, Multi-spectroscopic and molecular docking studies on the interaction of darunavir, a HIV protease inhibitor with calf thymus DNA, Spectrochim. Acta A 193 (2018) 14–22, https://doi.org/10.1016/j.saa.2017.11.061.
[49] M. Hu, M. Zhu, L. Xin, G. Zhang, S. Wu, X. Hu, et al., Change of benzo (a) pyrene during frying and its groove binding to calf thymus DNA, Food Chem. 350 (2021) 129276, https://doi.org/10.1016/j.foodchem.2021.129276.
[50] O.L. Kantidze, S.V. Razin, Weak interactions in higher-order chromatin organization, Nucleic Acids Res. 48 (9) (2020) 4614–4626, https://doi.org/10.1093/nar/gkaa261.
[51] B. Lindman, B. Medronho, L. Alves, M. Norgren, L. Nordenskiöld, Hydrophobic interactions control the self-assembly of DNA and cellulose, Q. Rev. Biophys. 54 (2021) e3, https://doi.org/10.1017/S0033583521000019.
[52] N. Luo, Y. Gao, M. Wang, X. Niu, G. Li, T. An, Bidirectional role of synthetic musk tonalide as photosensitizer and activator on amino acids: formation of sensitizer imine at aqueous chemistry interface of skin, Eco-Environ. Health 2 (1) (2023) 32–39, https://doi.org/10.1016/j.eehl.2023.03.002.
[53] J.L. Sims, K.M. Stroski, S. Kim, G. Killeen, R. Ehalt, M.F. Simcik, et al., Global occurrence and probabilistic environmental health hazard assessment of per- and polyfluoroalkyl substances (PFASs) in groundwater and surface waters, Sci. Total Environ. 816 (2022) 151535, https://doi.org/10.1016/j.scitotenv.2021.151535.